SCIENTIFIC REPORTS

OPEN

Unencapsulated Air-stable Organic Field Effect Transistor by All Solution Processes for Low Power Vapor Sensing

Received: 28 October 2015
Accepted: 11 January 2016
Published: 10 February 2016

Linrun Feng*, Wei Tang*, Jiaqing Zhao, Ruozhang Yang, Wei Hu, Qiaofeng Li, Ruolin Wang & Xiaojun Guo

With its excellent mechanical flexibility, low-cost and low-temperature processing, the solution processed organic field-effect transistor (OFET) is a promising platform technology for developing ubiquitous sensor applications in digital health, environment monitoring and Internet of Things. However, a contradiction between achieving low voltage operation and having stable performance severely hinder the technology to become commercially viable. This work shows that, by reducing the sub-gap density of states (DOS) at the channel for low operation voltage and using a proper low-*k* non-polar polymer dielectric layer, such an issue can be addressed. Stable electrical properties after either being placed for weeks or continuously prolonged bias stressing for hours in ambient air are achieved for all solution processed unencapsulated OFETs with the channel being exposed to the ambient air for analyte detection. The fabricated device presents a steep subthreshold swing less than 100 mV/decade, and an ON/OFF ratio of 10^6 at a voltage swing of 3V. The low voltage and stable operation allows the sensor made of the OFET to be incorporated into a battery-powered electronic system for continuously reliable sensing of ammonia vapor in ambient air with very small power consumption of about 50 nW.

Organic field-effect transistors (OFETs) have received worldly wide research attention, owning to their attractive features of sustainable performance improvement and functionalization through chemical structure tailoring, superior intrinsic mechanical flexibility, low temperature and fast processing, and compatibility with arbitrary substrates (plastic, paper and fabric)[1–6]. These features of OFETs ideally match well to ubiquitous sensors, which are demanded as part of global issue solutions for digital health, environment monitoring and Internet of Things[7–9]. The sensors, using OFETs as transducers, could be developed with low-cost and great freedom for sensing function integration on arbitrary substrates to work with multi-physics or bio/chemistry signals[10,11]. As opposed to other implementations such as a chemiresistor, OFET based sensors can provide better sensitivity through the amplification of the transistors[12–15]. However, most of these targeted sensor applications are portable or wearable, requiring the OFETs to be integrated in severely power-constraint electronic systems with battery or a. c. field. Good enough operational stability under electrical bias storage and lifetime are also prerequisites for practical use.

In the last decades, remarkable progresses have been made on development of high mobility soluble organic semiconductors[16,17], and solution or printing based fabrication techniques to develop a commercially competitive manufacturing approach for OFETs[18–20]. However, the demonstrated large operation voltage of typically a few tens volts, operational and storage instabilities in ambient air remain to be the main bottlenecks preventing further advances towards the targeted applications. Intensive studies have thus been made on improving the device stabilities[19–21] and reducing the operation voltage[22,23] for OFETs, respectively.

For OFETs in encapsulated or operated in inert environment, the bias stress effect (BSE) induced threshold voltage shift under continuous bias during operation is the most studied issue[24]. The main mechanism is thought to be the trapping of carriers from the gate bias-induced conduction channel into less mobile localized states[25]. The trapping probability is proportional to the local trap states, the gate induced electrical field strength and the

National Engineering Laboratory of TFT-LCD Materials and Technologies, Department of Electronic Engineering, Shanghai Jiao Tong University, Shanghai 200240, China. *These authors contributed equally to this work. Correspondence and requests for materials should be addressed to X.G. (email: x.guo@sjtu.edu.cn)

carrier density in the channel. Therefore, to reduce the BSE, it will be important to form a high quality semiconductor/dielectric interface. Weak gate electrical field and low carrier density during operation is also helpful. For OFETs in an unencapsulated structure, the channel layer is exposed to the ambient air. As a result, besides BSE, oxidative degradation of the semiconductor layer, and absorption of polar H_2O molecules on the semiconductor and the dielectric films can also happen to cause device degradation[26–28]. Therefore, for unencapsulated OFETs, to achieve the required long-term stability during storage and operation, air stable and water repellent semiconductor and dielectric materials are more urged. In the past, several air stable organic semiconductors have been developed by either modifying the side chains[29] or removing/blocking the oxidatively susceptible sites in the molecules[30]. It was also concluded from experiments that less polar dielectric free of -OH groups can effectively suppress water adsorption for better device stability[31–32].

On the other hand, to reduce the required operation voltage of OFETs, the widely used approach is to enlarge the gate dielectric capacitance with ultra-thin[33] or high-k[34] dielectric layer. However, a very thin dielectric layer is hard to be formed by simple printing or coating processes, and will cause large gate leakage current, and deteriorate the device functionality and reliability under electrical bias stress[35]. Moreover, a thin dielectric layer can also strengthen the gate electric field, and thus enhance charge trapping. For high-k gate dielectrics, the polar surface groups tend to trap carriers from gate bias induced conduction channel or interact with water from surrounding ambience if the devices are not well encapsulated[24]. The resulted localization of charge carriers or formation of Fröhlich polarons can cause not only mobility degradation[36], but also increased hysteresis and device instabilities[37]. As a result, a contradiction between achieving low voltage operation, and having stable device performance severely hinder solution processed OFETs to become commercially viable for the targeted ubiquitous sensor applications.

According to the field-effect transistor (FET) theory[38], the required voltage swing to switch a transistor is highly dependent on the subthreshold swing (S), which can be described as:

$$S = \ln\ 10 \cdot \frac{k_B \mathrm{T}}{q} \cdot \left(1 + \frac{q^2 N_{\mathrm{SS}}}{\mathrm{C_i}}\right) \tag{1}$$

where k_B is the Boltzman's constant, T is the absolute temperature, N_{SS} is the effective sub-gap DOS at the channel, q is the elementary charge, and C_i is the specific gate dielectric capacitance.

From equation 1, it can be seen that the required operation voltage for a FET depends on not only the gate dielectric capacitance, but also the effective sub-gap DOS at the channel. Therefore, if N_{SS} was effectively reduced, low voltage operation could also be realized. Our previous study reveals that, it is feasible to reduce the effective sub-gap DOS at the channel through blended solution of small molecule organic semiconductor and insulating polymer binder, and OFETs of steeper S can thus be realized for low voltage operation with less strict requirements on the capacitance of gate dielectric layer[39–42]. This work shows that, based on this material system to reduce the operation voltage, the contradiction between achieving low voltage operation and having stable device performance can be addressed for all solution processed OFETs by selecting a low-k non-polar polymer dielectric layer. The devices were implemented in a bottom-gate bottom-contact unencapsulated configuration, with the channel being exposed to the ambient air for analyte detection. Blend of small molecule acene semiconductor and insulating polymer binder was simply drop-casted on a thick and low-k poly(vinyl cinnamate) (PVC) gate dielectric layer to form a small sub-gap DOS channel without needing complex interface engineering processes. The source, drain and gate electrodes were formed by inkjet printed (IJP) silver.

The fabricated device presents a steep S less than 100 mV/decade, enabling an ON/OFF ratio of 10^6 with a voltage swing of 3 V. Even without encapsulation, the devices show very stable electrical properties after either being placed for weeks or continuously prolonged bias stressing for hours in ambient air. The excellent features of low voltage and stable operation allow the sensor tag made of the OFET to be incorporated into a self-designed 3.7 V lithium-battery powered electronic system for long-term reliable sensing of ammonia vapor in ambient air. The power consumption of the OFET sensor tag is as low as 50 nW.

Results

Device structure and processes. Figure 1(a) illustrates the bottom gate bottom contact (BGBC) device structure of the fabricated OFETs with the channel being exposed to the ambient air for analyte detection. The photo image of an array of OFETs fabricated on 6 cm × 6 cm size polyethylene naphthalate (PEN) substrate is given in Fig. 1(b). Silver gate, source and drain electrodes are formed by IJP of metal-organic precursor type ink, followed by a 15 min annealing process at 145 °C. A 295 nm thick non-polar PVC film (dielectric constant of 3.4) is used as the gate dielectric layer, resulting in a dielectric capacitance of 10.2 nF/cm^2 at 20 Hz. The sample was then placed on an inclined support (a glass slide with the tilt angle of 10°), and blend of 6,13-bis(triisopropylsilylethynyl)-pentacene (TIPS-pentacene) and polystyrene (PS) in chlorobenzene is drop casted on the surface of the source-drain contacts and the PVC dielectric layer using a micropipette to form the semiconductor layer. The inclined structure help to form long crystalline TIPS-pentacene domains oriented along the channel[43], as shown in Fig. 1(c). The X-ray diffraction (XRD) spectrum in Fig. 1(d) shows high diffraction peaks at 5.56°, 10.9° and 16.28°. The spectrum agrees well with previously reported results, indicating well-ordered triclinic structure of the formed semiconductor film[44].

Low voltage operation. Figure 2(a,b) show the measured representative transfer and output characteristics of the devices. Despite the small specific gate dielectric capacitance of 10.2 nF/cm^2 as shown in Fig. S1(a), the device presents a steep S as small as 97 mV per decade. The gate leakage current is favoritely low attributed to the relatively thick polymer dielectric layer. The extracted values of S and ON/OFF current ratio from the transfer characteristics for 15 devices over a 6 cm × 6 cm size substrate (Fig. S1(b)) are given in Fig. 2(c). The extracted

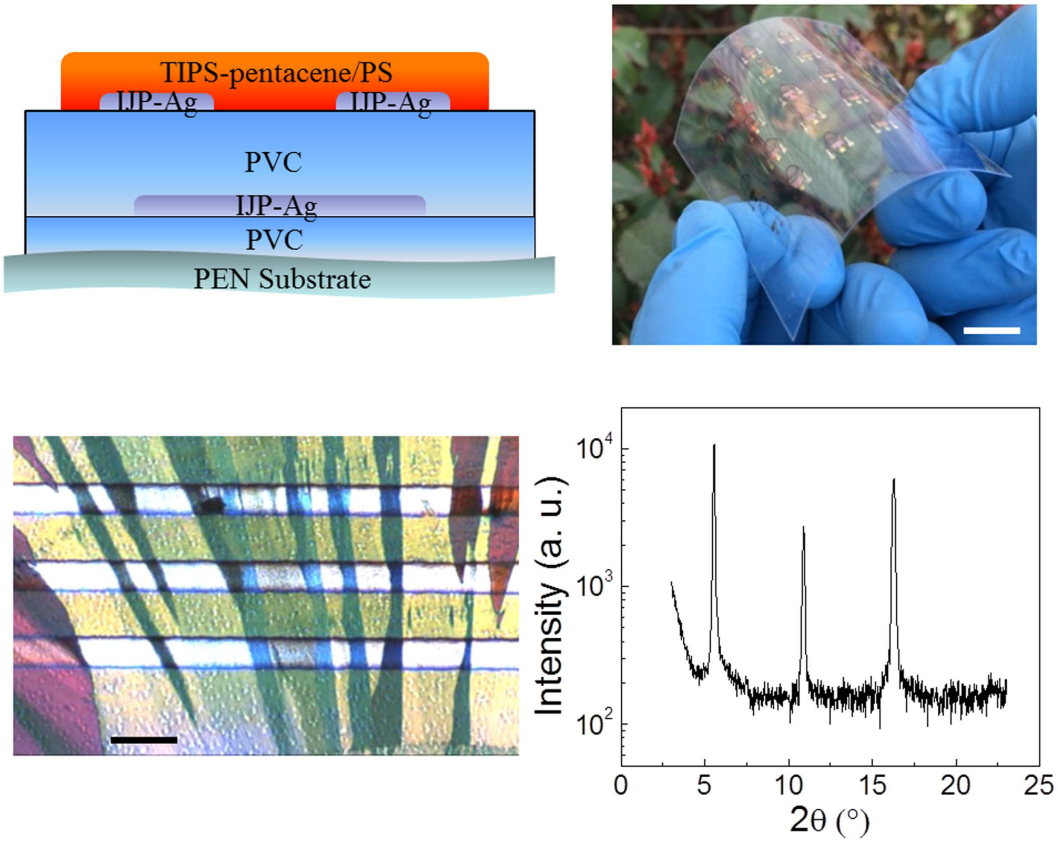

Figure 1. Device structure of the fabricated all solution processed OFETs. (**a**) The schematic diagram of the fabricated bottom gate bottom contact OFET devices. (**b**) The photo image of the 6 cm × 6 cm flexible sample. The scale bar is 1 cm. (**c**) The top-view polarized optical micrograph of the channel area for the device. The scale bar is 100 μm. (**d**) The X-ray diffraction (XRD) spectrum of the semiconductor for the device.

mobility and threshold voltage (V_{th}) values for the 15 devices are given in Fig. S1(c). The relatively thick (295 nm) gate dielectric layer help to achieve good yield for the low voltage devices even when all processes were completed in a non-cleanroom lab environment. The field-effect mobility in the saturation regime, μ_{sat}, is extracted to be around 0.6 $cm^2/(V.s)$, using the expression $\mu_{sat} = 2L/WC_i(\partial\sqrt{ID}/\partial V_{GS})^2$ at a gate-source voltage of −3 V, where I_D is the drain current, V_{GS} is the gate-source voltage, C_i is the specific gate dielectric capacitance, and L and W are the channel length and width, respectively. As shown in Fig. S2, the mobility value is normal for TIPS-pentacene based devices, but is extracted at a much lower gate electrical field. The deep S, low gate leakage and high mobility enable to achieve an ON/OFF current ratio of 10^6 with a voltage swing of 3 V. It can be seen from Table 1 that, in terms of the achieved ON/OFF ratio and the required voltage swing, the device in this work presents the best performance among all solution processed OFETs, which is even comparable with all vacuum processed low voltage OFETs with a nanometer scale thick inorganic gate dielectric layer[45]. The performance is attributed to much lower effective sub-gap DOS at the channel, which is of orders lower than previous work[34,45–50], as compared in Table 1. The effective sub-gap DOS N_{ss} is extracted based on equation 1.

The exhibited negligible hysteresis in both output and transfer characteristics also indicates low trap interfaces formed between the semiconductor layer and the gate dielectric layer, and the semiconductor layer and the ambient air. These high quality interfaces are prerequisites for achieving stably operated OFETs.

Operational and shelf lifetime stabilities. For practical sensor applications, both operational and storage stabilities and under continuous electrical bias are required. The measured transfer electrical characteristics and the relative changes of extracted mobility and threshold voltage over time are given in Fig. 3(a,b), showing very stable performance under continuous bias stress at $V_{GS} = V_{DS} = -5$ V for 25000 seconds. It should be noted that such bias conditions represent the worst case for sensor applications, since for most of cases, the OFET will be biased with smaller voltages and in turn a less current density, as discussed later. Continuous bias stress was also performed for other three devices, which presented similarly good bias stress stabilities in the ambient air as shown in Fig. S3. The fabricated devices without any encapsulation were stored in an uncontrolled environment for four weeks with the recorded humidity and temperature given in Fig. S4(a). The transfer electrical characteristics were measured during the storage, as shown in Fig. 3(c), and the extracted relative changes of mobility and threshold voltage over time are given in Fig. 3(d). The results show stable electrical properties of the device during storage in ambient air. The measurement results for all measured three devices in Fig. S4(b) well prove the reproducibility.

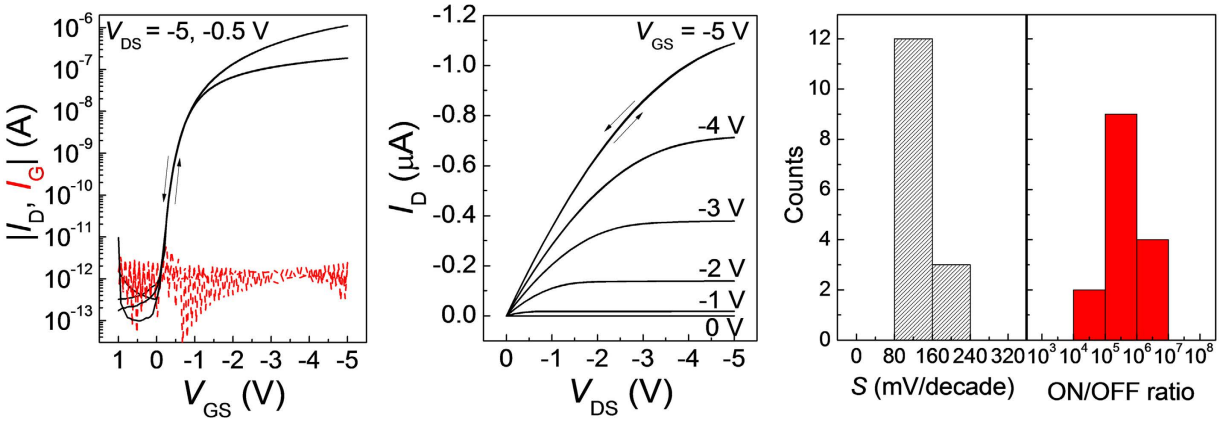

Figure 2. The measured representative electrical characteristics of the fabricated device with the channel length of 80 μm and channel width of 1600 μm. (**a**) Transfer characteristic ($I_D - V_{GS}$), (**b**) Output characteristic ($I_D - V_{DS}$) and (**c**) The histograms of extracted subthreshold swing (*S*) and ON/OFF current ratio for 15 devices over a 6 cm × 6 cm size substrate.

Work	Gate Dielectric	Thickness [nm]	C_i [nF/cm^2]	Semiconductor	Source/Drain Electrodes	Substrate	ON/OFF Ratio	Voltage Swing [V]	N_{SS} [eV^{-1}cm^{-2}]
34	P(VDF-TrFE-CFE) (SP)	160	330	PBTTT (SP)	Au (VP)	Glass	10^6	2.5	1.4×10^{12}
45	ODPA/AlOx (SP/VP)	2.1/3.6	700	Pentacene (VP)	Au (VP)	Glass	10^6	2	3.0×10^{12}
46	Cytop (SP)	900	2.1	TIPS-pentacene (SP)	Au (VP)	Glass	10^6	60	5.6×10^{11}
47	D207 (SP)	360	6.9	S1200 (SP)	Ag (SP)	Parylene	10^6	6	3.9×10^{11}
48	Teflon (SP)	200	8.4	diF-TES-ADT (SP)	Ag (SP)	PEN	10^6	25	9.8×10^{11}
49	PVP (SP)	900	3.8	TIPS-pentacene (SP)	Ag (SP)	Polyarylate	10^5	60	9.7×10^{11}
50	ODPA/AlOx (SP/VP)	2.5/4	450	TIPS-Pentacene (SP)	Au (VP)	p^{++} Si Wafer	10^6	2	1.91×10^{12}
Our work	PVC (SP)	295	10.2	TIPS-Pentacene (SP)	Ag (SP)	PEN	10^6	3	3.9×10^{10}

Table 1. Comparisons of ON/OFF ratio, the voltage swing, and the extracted N_{SS} at the semiconductor/dielectric interface for our work and other OFETs. Note: SP, solution processed; VP, vacuum processed; D207, Merck lisicon D207; S1200, Merck lisicon S1200; diF-TES-ADT, 2,8-difl uoro-5,11-bis(triethylsilylethynyl) anthradithiophene; PEN, polyethylene naphthalate; PVP, poly-4-vinylphenol; TIPS-Pentacene, 6,13(bis-triisopropylsilylethynyl) pentacene; P(VDF-TrFE-CFE), poly(vinylidene fluoride-trifluoroethylene-chlorofluoroethylene) PBTTT, poly(2,5-bis(3-dodecylthiophene-2-yl)thieno[3,2-b]thiophenes); ODPA, n-octadecylphosphonic acid; PVC, poly (vinyl cinnamate).

The results prove stable electrial properties of the devices during storage in ambient air. The device stability performance in this work is the best among all reported solution processed or printed OFETs, and is even comparable to previous work with well designed encapsulation[22]. The excellent stabilities are attributed to the air stable and water repellent semiconductor layer and the dielectric materials used in the device. TIPS-pentacene has shown to be an air stable organic semiconductor material with a deep LUMO level of −3.42 eV, and functional groups at the 6 and 13 positions of the molecule protecting the central aromatic ring from oxidation[51–53]. The deposited film from blend of TIPS-pentacene and PS is hydrophobic to be water repellent with a measured water contact angle of 103° as shown in Fig. S5. Blending of small molecule organic semiconductor such as TIPS-pentacene with insulating polymer binder has been reported to be able to improve the crystallization control to obtain a highly crystalline thin film channel[39,46,54]. As a result, a high quality semiconductor/dielectric interface of low trap states can be formed, which is also important to reduce bias stress induced instabilities.

To prove the importance of the gate dielectric on the device stabilities, devices in the same structure but with PVC and polyvinyl alcohol (PVA) as the gate dielectric layer, respectively, were fabricated on glass substrates for stability comparison, as shown in Fig. S6. It can be seen that both devices present similar low voltage operation properties, indicating the approach for low voltage operation is applicable to different gate dielectric materials. However, since the polar PVA film contains hydroxyl groups (-OH groups) and easily absorbs water, as shown in Fig. S7, the devices present much poorer operational and storage stabilities than the devices with a PVC gate dielectric layer.

The excellent operational and storage stabilities enable using the channel of the OFET as the sensitive layer for long-term reliable vapor or gas sensing without needs of complicated design such as differential sensing architecture[55,56].

Demonstration of ammonia sensing. NH_3 sensing in ambient air environment is taken as an example to examine the feasibility of integrating the fabricated low voltage and stable OFET in a low power electronics

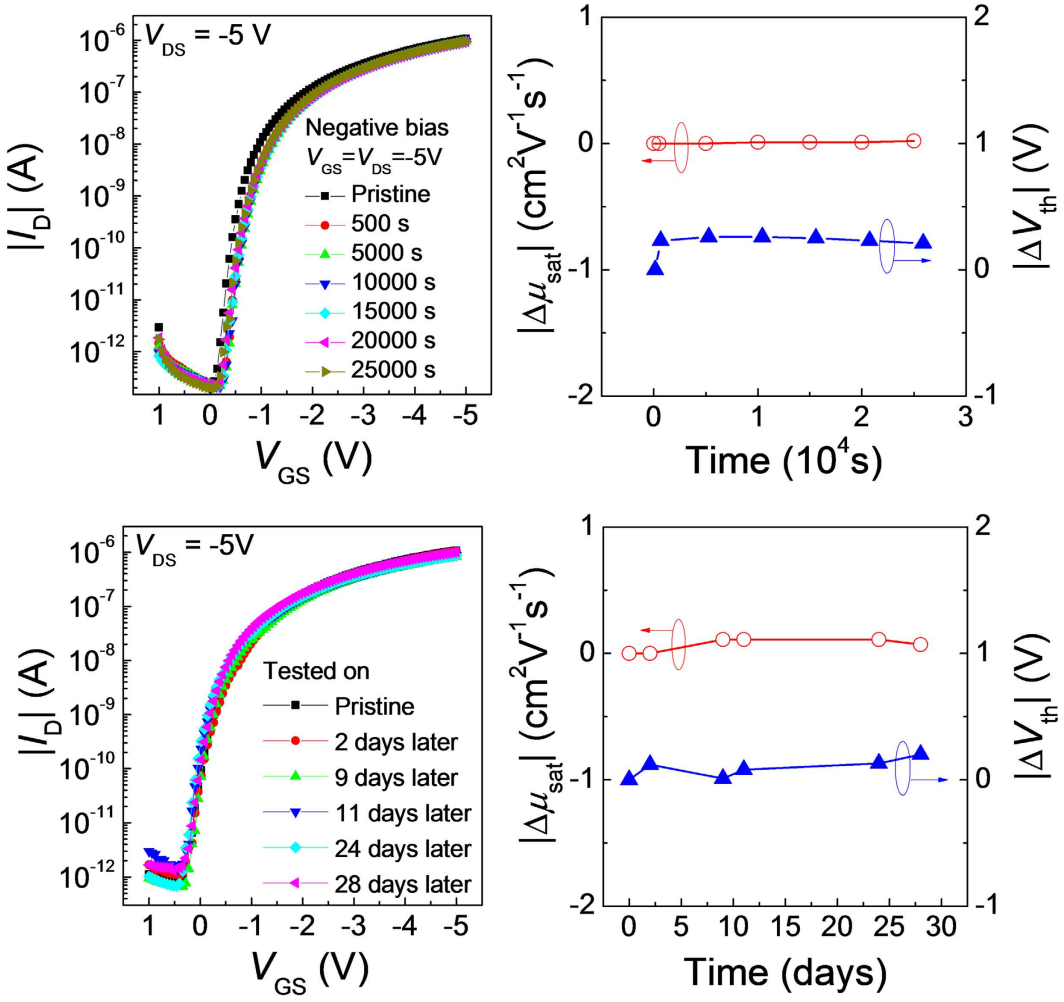

Figure 3. Operational and shelf lifetime stabilities of OFETs. (**a**) The measured bias stress stability of the device with an applied bias voltage of $V_{GS} = V_{DS} = -5$ V for 25000 s. (**b**) The relative changes of extracted mobility and threshold voltage of the devices as a function of bias time. (**c**) The measured transfer characteristics of the device during the four weeks' storage in ambient air environment. (**d**) The relative changes of extracted mobility and threshold voltage of the devices as a function of time. The relative humidity and temperature at each measurement over the four week are given in Fig. S4(a).

system for reliable sensing. The measured $I_D - V_{GS}$ characteristics in ambient air without NH_3 exposure, upon NH_3 exposure and removal of NH_3 exposure, are compared in Fig. S8. Upon NH_3 exposure, there is significant change of the $I_D - V_{GS}$ curve with a negative V_{th} shift of 0.25 V, and a decrease in mobility from 0.6 cm^2/(V.s) to 0.3 cm^2/(V.s). NH_3 has large dipole moment of about 1.46 debye. When NH_3 molecules are absorbed (mostly at the grain boundaries[57]), the dipolar nature of the NH_3 molecule produces an electric field capable of strongly binding mobile charges. Then more charges will have to be injected into the active layer in order to turn on the device, which means a negative shift in V_{th} for a p-type OFET. Moreover, the dipolar nature of NH_3 induced charge-dipole interactions is likely to degrade the charge transport in the channel by increasing energetic disorders[58,59], which in turn reduces the field-effect mobility. Upon removal of the analyte, the $I_D - V_{GS}$ curve is almost completely restored to its original condition, indicating that the NH_3 analyte molecules interact with the semiconductor film surface through weak physical absorption (Van del Waals force). After initial studies of its recoverable response to the NH_3 analyte, the fabricated OFET sensor tag was integrated into a self-designed battery powered readout system to evaluate the long-term sensing performance. The supply voltage (V_{DD}) of the OFET sensor tag is 2.4 V. The circuit schematic of the whole system including the OFET sensor tag and the readout circuit board is illustrated in Fig. 4(a). The drain current of the OFET is converted to a voltage output signal (V_{out}) through a load resistor (R_L) in the circuit board, which is then processed by the circuit blocks including a voltage follower and a 12 bit analog-to-digital converter (ADC). The obtained data are stored in the embedded memory in the MCU for collection, and can also be displayed on a liquid crystal display (LCD) screen in real time through a digital I/O interface. The measured voltage transfer curve between V_{out} and the bias voltage at the gate of the OFET (V_{in}) is given in Fig. 4(b). V_{in} is set as the value to achieve the maximum voltage gain. The DC power consumption (P_{DC})

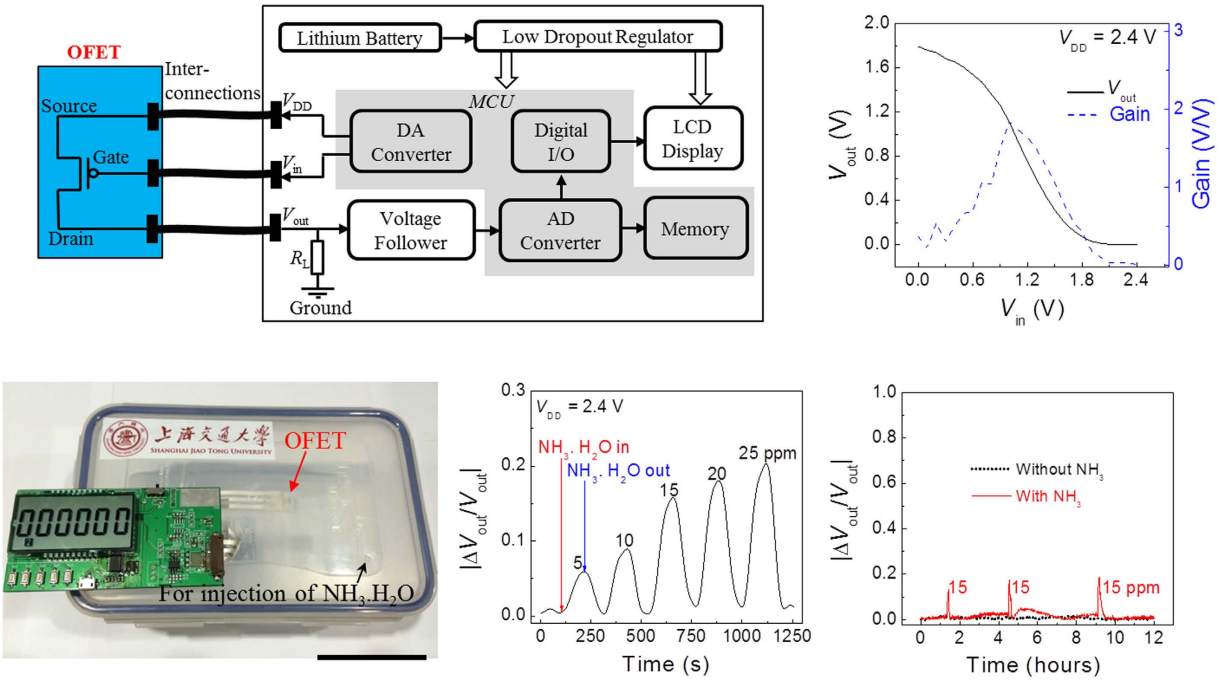

Figure 4. Demonstration of ammonia sensing. (**a**) The circuit schematic of the test system including the OFET sensor tag and the readout circuit board. (**b**) The measured voltage transfer curve between the V_{out} and V_{in}, the bias voltage of V_{in} during the NH_3 test is set as the value to achieve the maximum voltage gain. (**c**) The photograph of the test system. The sensor tag was placed in a plastic container and connected to the test board with a plastic strip. The ammonia water is directly injected into the container via a hole on the top of it. The scale bar is 5 cm. (**d**) The measured relative change of V_{out} over time upon NH_3 exposure of different estimated concentrations from 5 ppm to 25 ppm. (**e**) Long-term sensing performance of the OFET for 12 hours' continuous test with the system.

of the OFET sensor tag can be estimated to be around 50 nW ($P_{DC} \approx V_{DD} \times I_D$), which is the lowest reported value among all reported OFET based sensors[60–63].

To evaluate the performance for long-term NH_3 sensing in ambient air, the OFET sensor tag was placed in a plastic container and connected to the readout circuit board outside through a plastic conductive strip, as illustrated in Fig. 4(c). Delivery of the analyte into the container is through direct injection of ammonia water ($NH_3.H_2O$) using a micropipette via a hole on top of the container. The concentration of NH_3 in the container can be roughly estimated according to the volume of the container, the amount of the injected $NH_3.H_2O$ and its concentration as described in the Experimental part. The detected concentration should be less than the estimated value, since the NH_3 molecules might not distribute evenly in the container with the upper region of the container, where the sensor is located, having lower concentration than the bottom part. The sensor tag was taken out of the container for removal of the analyte exposure. A video recording the whole procedure is given in the Supplementary. Fig. 4(d) shows the response of the detected signal over time upon NH_3 exposure of different estimated concentrations from 5 ppm to 25 ppm. The device shows relatively fast response upon the NH_3 exposure and removal of the exposure. The response time is also related to the volatilization and diffusion speed of NH_3 molecules after the ammonia water is injected into the container. Nearly full recovery for all test cycles prove the re-usable feature of the device, which is attributed to weak physical absorption of the analyte to the semiconductor layer surface as mentioned above. Long-term sensing performance was characterized further by continuous test of the OFET for 12 hours with the system. A fixed amount of amonnia water (20 μL) was injected into the container for three times during the period, corresponding to an estimated concentration of 15 ppm. The sensor tag was taken out of the container and then put back after each injection. A same system being running simultaneously without injection of ammonia water was used as the reference. Figure 4(e) shows the test results for the sensor system with repeated NH_3 exposures, and the reference one being run without exposure to NH_3. It can be seen that, the OFET sensor is very stable without NH_3 in the ambient air. The results prove the capability of the device for long-term reliable vapor or gas sensing in ambient air.

Discussions

Due to material and process constraints, there is a hurdle to achieve both low voltage operation and good stabilities for printable OFETs, especially in an unencapsulated structure. The approach of reducing the sub-gap DOS at the channel is proved to be an effective way to break this deadlock. Based on this idea, a thick low-*k* non-polar polymer dielectric layer, which has a wide range of material choices, can be used to realize low voltage OFETs with better compatibility with printing processes. It is also shown that both storage and operation instability issues can be addressed by using air stable and water repellent semiconductor and dielectric materials. The fabricated

devices with IJP Ag electrodes present a steep S less than 100 mV/decade and a high ON/OFF current ratio larger than 10^6, which can help to achieve large detection range for sensing in the subthreshold regime, when the device interfaces with low voltage signal processing silicon chips. The low voltage and also low current density properties of the OFETs results in ultra-low DC power consumption of the sensor tag at the level of around 50 nW during operation, which is the lowest among all reported OFET based sensors, and is attractive for mobile or wearable applications[64]. The demonstration of the OFET being operated in a low voltage battery powered electronic system for long-term and repeatable sensing of the NH_3 exposure prove the above excellent features of the devices and the capability for practical applications. Moreover, the semiconductor material (blend of TIPS-pentancene and PS), the gate dielectric material (PVC) and the Ag ink used in this work are all commercially available, showing great potential of the technology to be commercially competitive. The work also indicates the importance of engineering the device design with available materials for development of OFET technology.

In conclusion, by reducing the sub-gap DOS at the channel, this work develops fully printable low voltage OFETs with ultra-low power and excellent device stabilities during storage and operation. The first demonstration of an OFET being operated in a battery powered low voltage electronic system for long-term and reliable vapor sensing well prove the device design to be an ideal solution to address the issues with printable OFETs. This work would open a new route to develop a commercially viable printed OFET technology platform for ubiquitous sensor applications.

Experimental

Materials and device fabrication. The structure of the fabricated bottom-gate bottom-contact (BGBC) OFETs on flexible substrate is illustrated in Fig. 1(a). A 125-μm-thick polyethylene naphthalate (PEN) foil of 6 cm × 6 cm size was used as the substrate. Poly(vinyl cinnamate) (PVC) solution in chlorobenzene at a concentration of 50 g/L was spin-coated onto the substrate at 3000 r/min, followed by a cross-linking process through UV treatment (UV Curer KW-4AC) for 20 min and then heating at 100 °C for 1 hour, to form the planarization layer. The wavelength of UV radiation was 254 nm. The molecular weight (M_W) of used PVC is 95000. Gate electrodes were printed onto the planarization layer from a type of metal-organic precursor Ag ink (Jet-600C, Hisense Electronics) using a piezoelectric inkjet printer (DMP2831, Dimatix) with a 10 pL cartridge. The cartridge temperature was maintained at 40 °C, while the plate was kept at room temperature. The drop space and print height were set to be 40 μm and 0.8 mm, respectively. The printed Ag gate was sintered at 145 °C for 15 min in the ambient air. Then the same processes as that for the planarization layer were used to deposit the PVC gate dielectric layer. The source/drain electrodes were formed using the same process for the gate electrodes, defining the channel length and width of 80 μm and 1600 μm, respectively. Subsequently, the source/drain electrodes were modified with self-assembled-monolayer (SAM) by immersing the sample in a 5×10^{-3} mol/L solution of perfluorobenzenethiol (PFBT) in ethanol for 2 min and then rinsed with ethanol. The surface of Ag electrodes was treated by PFBT to form good contacts with the organic semiconductor[65]. Before depositing the semiconductor layer, the sample was placed on a glass slide as an inclined support to form a tilted angle of 10°. The semiconducting layer was finally deposited by drop-casting a solution made by mixing 6,13-bis(triisopropylsilylethynyl)-pentacene (TIPS-pentacene) and polystyrene (PS) at 10 mg/ml concentration of solids in chlorobenzene (3:1 ratio by volume), followed by an annealing process at 100 °C for 30 min in ambient air environment. The M_W of used PS is 524000. All the processes were completed in a non-cleanroom lab environment.

Material and device characterization. The polarized optical micrograph was taken with a Cakon-XPF-300C microscope. X-ray diffraction (XRD) spectrum of the semiconductor film was characterized with Bruker-AXS D8 Advance system. The surface roughness was measured using a BioScope Veeco atomic force microscope. A WK6515B precision impedance analyzer was used for capacitance measurement. Film thickness was characterized by a KLA-Tencor D-120 Stylus Profiler. The contact angle measurement was carried out with a Solon-200B contact-angle analyser. The electrical properties of the devices were tested with a Keithley 4200 semiconductor characterization system. All measurements were performed at room temperature in ambient air environment.

Readout circuit board. The circuit schematic of the test system including the OFET sensor tag and the readout circuit board is illustrated in Fig. 4(a). The drain current of the OFET is converted to a voltage output signal (V_{out}) through a load resistor (R_L) in the circuit board, the R_L is 50 MΩ. Before processed by MCU, the V_{out} is buffered by an operational amplifier Microchip MCP6002, which is connected and used as a voltage follower. The analog-to-digital conversion of V_{out} is performed with a 12 bit analog-to-digital converter (ADC) in Texas Instruments MCU MSP430F2618. The digital data V_{out} is then stored in the embedded memory of MCU. In parallel, the data is also displayed on a liquid crystal display (LCD) screen in real time through a digital I/O interface. A Holtek HT1621 is used as the LCD driver.

The MCU and LCD are powered by a 3.7 V lithium battery through a low dropout regulator Texas Instruments LP2982. The operation voltage of the MCU and LCD is 3.3 V, which is provided by the low dropout regulator. The supply voltage (V_{DD}) and bias voltage (V_{in}) of OFET are provided by the digital-to-analog converter (DAC) of MCU.

Source code written in C programming language is used to control the whole readout circuit board.

NH_3 sensing system. The photograph of the NH_3 test system is shown as Fig. 4(c). A 1.2 L plastic container was used as the test chamber. The OFET sensor tag was cut from the 6 cm × 6 cm flexible sample with a scissor. The tag was placed in the plastic container and connected to the readout circuit board outside through a plastic conductive strip. The plastic conductive strip was fabricated by dispensing three lines of silver paste on polyethylene terephthala (PET), followed by heating at 110 °C for 20 min. The width, length and space between each other

of the conductive silver lines were 2 mm, 100 mm and 2 mm, respectively. The OFET sensor tag was attached to one side of the plastic conductive strip with double-sided tape. Then the gate/source/drain electrode of OFET sensor tag was connected to each conductive silver line on the conductive strip by dispensing silver paste, followed by heating at 100 °C for 20 min. The other side of conductive strip was connected with readout circuit board through a Flexible Flat Cable (FFC) socket.

Delivery of the analyte into the container is through direct injection of $NH_3.H_2O$ using a micropipette via a hole on top of the container, the hole will be covered with a transparent tape after the injection. During the test, 20 μL of $NH_3.H_2O$ with corresponding concentration was injected into the container. The concentration of NH_3 (C_{NH3}) in the container can be roughly estimated as:

$$C_{NH_3}(ppm) = \frac{\rho \times V \times \omega}{M} \times \frac{V_m}{V_c} \times 10^6 \quad (2)$$

where ρ (0.91 g/mL) is the density of $NH_3.H_2O$, V (20 μL) is the volume of the injected $NH_3.H_2O$, ω is the mass ratio of the NH_3 in $NH_3.H_2O$, M (17 g/mol) is the molar mass of NH_3, V_m (22.4 L/mol) is the molar volume of ideal gas, and V_c (1.2 L) is the volume of the plastic container. Assuming that NH_3 distributes evenly in the container after the injection, a 20 μL $NH_3.H_2O$ with ω of 0.075% corresponds to a concentration of 15 ppm.

References

1. Venkateshavaran, D. *et al.* Approaching disorder-free transport in high-mobility conjugated polymers. *Nature* **515,** 384–388 (2014).
2. Kaltenbrunner, M. *et al.* An ultra-lightweight design for imperceptible plastic electronics. *Nature* **499,** 458–463 (2013).
3. Sirringhaus, H. 25th anniversary article: Organic field-effect transistors: the path beyond amorphous silicon. *Adv. Mater.* **26,** 1319–1335 (2014).
4. Giri, G. *et al.* Tuning charge transport in solution-sheared organic semiconductors using latice strain. *Nature* **480,** 504–508 (2011).
5. Minemawari, H. *et al.* Inkjet printing of single-crystal films. *Nature* **475,** 364–367 (2011).
6. Sekitani, T. *et al.* Organic nonvolatile memory trasistors for flexible sensor arrays. *Science* **11,** 1516–1519 (2009).
7. Knopfmacher, O. *et al.* Highly stable organic polymer field-effect transistor sensor for selective detecion in the marine environment. *Nat. Commn.* **5,** 2954 (2014).
8. Spanu, A. *et al.* An organic transistor-based system for reference-less electrophysioloical monitoring of excitable cells. *Sci. Rep.* **5,** 8807 (2015).
9. Lin, P. *et al.* Organic thin-film transistors for chemical and biological sensing. *Adv. Mater.* **24,** 34–51 (2012).
10. Mannsfeld, S. *et al.* Highly sensitive flexibe pressure sensors with microstructured rubber dielectric layers. *Nat. Mater.* **9,** 859–864 (2010).
11. Mulla, M. *et al.* Capacitance-modulted transistor detects odorant binding protein chiral interactions. *Nat. Commun.* **6,** 6010 (2015)
12. Zhan, Y. *et al.* Flexible suspended gate organic thin-film transistors for ultra-sensitive pressure detection. *Nat. Commun.* **6,** 6269 (2015).
13. Zhang, M. *et al.* Highly sensitive glucose sensors based on enzyme-modified whole-graphene solution-gated transistors. *Sci. Rep.* **5,** 8311 (2014).
14. Lee, M. *et al.* Highly sensitive and selective liquid-phase sensors based on a solvent-resistant organic-transistor platform. *Adv. Mater.* **27,** 1540–1546 (2015).
15. Torsi, L. *et al.* A sensitivity-enhanced field-effect chiral sensor. *Nat. Mater.* **7,** 412–417 (2008).
16. Li, J. *et al.* A stable solution-processed polymer semiconductor with record high-mobility for printed transistors. *Sci. Rep.* **2,** 754 (2012).
17. Kim, G. *et al.* A thienoisoindigo-naphthalene polymer with ultrahigh mobility of 14.4 $cm^2/V{\cdot}s$ that substantially exceeds benchmark values for amorphous silicon semiconductors. *J. AM. Chem. Soc.* **136,** 9477–9483 (2014).
18. Chang, J. *et al.* Controlled growth of large-are high-performance small-molecule organic single-crystalline transistors by slot-die coating using a mixed solvent system. *Adv. Mater.* **25,** 6442–6447 (2013).
19. Diao, Y. *et al.* Solution coating of large-area organic semiconductor thin films with aligned single-crystalline domains. *Nat. Mater.* **12,** 665–671 (2013).
20. Kim, S. *et al.* Ink-jet-printed organic thin-film transistors for low-voltage-driven CMOS circuits with solution-processed AlO_x gate insulator. *IEEE Electron Device Lett.* **34,** 307–309 (2013).
21. Park, Y. *et al.* Room-temperature fabrication of ultrathin oxide gate dielectric for low-voltage operation of organic field-effect transistors. *Adv. Mater.* **23,** 971–974 (2011).
22. Hwang, K. *et al.* Top-gate organic field-effct transistors with high environmental and operational stability. *Adv. Mater.* **23,** 1293–1298 (2011).
23. Umeda, T. *et al.* High air-stability of threshold voltage on gate bias stress in pentacene TFTs with a hydroxyl-free and amorphous fluoropolymer as gate insulators. *Org. Electron.* **9,** 545–549 (2008).
24. Sirringhaus, H. Reliability of organic field-effect transistors. *Adv. Mater.* **21,** 3859–3873 (2009).
25. Lee, W. *et al.* 25th anniversary article: Microstructure dependent bias stability of organic transistors. *Adv. Mater.* **26,** 1660–1680 (2014).
26. Benor, A. *et al.* Electrical stability of pentacene thin film transistors. *Org. Electron.* **8,** 749–758 (2007).
27. Li, D. *et al.* Humidity effect on electrical performance of organic thin-film transistors. *Appl. Phys. Lett.* **86,** 042105 (2005).
28. Kumai, D. *et al.* Influence of H_2O and O_2 on threshold voltage shift in organic thin-film transistors: Deprotonation of SiOH on SiO_2 gate-insulator surface. *Appl. Phys. Lett.* **92,** 093309 (2008).
29. Takimiya, K. *et al.* Thienoacene-based organic semiconductors. *Adv. Mater.* **23,** 4347–4370 (2011).
30. Anthony, J. *et al.* A road map to stable, soluble, easily crystallized pentacene derivatives. *Org. Lett.* **4,** 15–18 (2002).
31. Lee, S. *et al.* Effects of hydroxyl groups in polymeric dielectrics on organic transistor performance. *Appl. Phys. Lett.* **88,** 162109 (2006).
32. Zan, H. *et al.* Stable encapsulated organic TFT with a spin-coated poly(4-vinylphenol-co-methyl methacrylate) dielectric. *IEEE Electron Device Lett.* **32,** 1131–1133 (2013).
33. Wöbkenberg, P. *et al.* Low-voltage organic transistor based on solution processed semiconductos and self-assemble monolayer gate dielectrics. *Appl. Phys. Lett.* **93,** 013303 (2008).
34. Li, J. *et al.* Solution processable low-voltage organic thin film transistors with high-*k* relaxor ferroelectric polymer as gate insulator. *Adv. Mater.* **24,** 88–93 (2012).
35. Cheng, X. *et al.* Air stable cross-linked Cytop ultrathin gate dielectric for high yield low-voltage top-gate organic field-effect transistors. *Chem. Mater.* **22,** 1559–1566 (2010).
36. Veres, J. *et al.* Low-*k* insulators as the choice of dielectrics in organic field-effect transistors. *Adv. Funct. Mater.* **13,** 199–204 (2003).

37. Park, D. *et al.* Low hysteresis pentacene thin-film transistors using SiO_2/cross-linked poly (vinyl alcohol) gate dielectric. *Appl. Phys. Lett.* **89,** 263507 (2006).
38. Sze, S. *et al.* In *Physics of Semiconductor Devices*, Vol. 3, Wiley-VCH, Germany (2007).
39. Feng, L. *et al.* Ultralow-voltage solution-processed organic transistors with small gate dielectric capacitance. *IEEE Electron Device Lett*. **34,** 129–131 (2013).
40. Li, S. *et al.* Application of thermal azide-alkyne cycloadditin (TAAC) reaction as a low temperature cross-linking method in polymer gate dielecrics for organic field-effect transistors. *J. Mater. Chem. C.* **2,** 3517–2520 (2014).
41. Tang, W. *et al.* Inkjet printed fined silver electrodes for all-soltion processed low-voltage organic thin film transistors. *J. Mater. Chem. C.* **2,** 1995–2000 (2014).
42. Li, S. *et al.* Low temperature cross-linked high performance polymer gate dielectrics for solution processed organic field-effect transistors. *Polym. Chem*. **6,** 5884–5890 (2015).
43. Lee, W. *et al.* Solution-processable pentacene microcrystal arrays for high performance organic field-effect transistors. *Appl. Phys. Lett.* **90,** 132106 (2007).
44. Park, S. *et al.* High mobility solution processed 6,13-bis (triisopropyl-silylethynyl) pentacene orgnic thin film transistors. *Appl. Phys. Lett*. **91,** 063514 (2007).
45. Klauk, H. *et al.* Ultralow-power organic complementary circuits. *Nature* **445,** 745–748 (2007).
46. Hamilton, R. *et al.* High-performance polymer-small molecule blend organic transistors. *Adv. Mater*. **21,** 1166–1171 (2009).
47. Fukuda, K. *et al.* Fully-printed high-performance organic thin-film transistors and circuitry on one-micron-thick polymer films. *Nat. Commun.* **5,** 4147 (2014).
48. Pierre, A. *et al.* All-printed flexible organic transistors enabled by surface tension-guided blade coating. *Adv. Mater*. **26,** 5722–5727 (2014).
49. Chung, S. *et al.* All-inkjet-printed organic thin-film transistor inverter on flexible plastic substrate. *IEEE Electron Device Lett*. **32,** 1134–1136 (2011).
50. Acton, O. *et al.* Spin-cast and patterned organophosphonate self-assembled monolayer dielectrics on metal-oxide-activated Si. *Adv. Mater*. **26,** 1899–1902 (2011).
51. Park, S. *et al.* Environmental and operatioal stability of solution-processed 6,13-bis (triisopropyl-silylethynyl) pentacene thin film transistors. *Org. Electron*. **10,** 486–490 (2009).
52. Kaur, I. *et al.* Substiuent effects in pentacenes: Gaining conrol over HOMO-LUMO gaps an photooxidative resistcs. *J. Am. Chem. Soc*. **130,** 16274–16286 (2008).
53. Maliakal, A. *et al.* Photochemical stability of pentacene ad substituted pentacen in solution and in thin films. *Chem. Mater*. **16,** 4980–4986 (2004).
54. Kang, J. *et al.* Structure and properties of small molecule-polymer blend semiconductors for organic thin film transistors. *J. Am. Chem. Soc.* **130,** 12273–12275 (2008).
55. Manoli, K. *et al.* Pulsed voltage driven organic field-effect transistors for high stability transient current measureents. *Org. Electron.* **15,** 2372–380 (2014).
56. Mirza, M. *et al.* Novel top-contact monolayer pentacene-based thin-film transistor for ammonia gas detection. *ACS Appl. Mater. Interfaces* 6, 5679–5684 (2014).
57. Yu, X. *et al.* Flexible spray-coated TIPS-pentacen organic thin-film transistors as ammonia gas sensors. *J. Mater. Chem. C.* **1,** 6532–6535 (2013).
58. Yu, J. *et al.* Ammonia gas sensor based on pentacene oganic field-effect transistor. *Sens. Actuators B*. **173,** 133–138 (2012).
59. Jeong, J. *et al.* The response characteristics of a gas sensor based on poly-3-hexylithiophene thin-film transistors. *Sens. Actuators B.* **146,** 40–45 (2010).
60. Zhang, C. *et al.* Organic field-effect transistor-based gas sensors. *Chem. Soc. Rev*. **44,** 2087–2107 (2015).
61. Torsi, L. *et al.* Organic field-effect transistor sensors: a tutorial review. *Chem. Soc. Rev*. **42,** 8612–8628 (2013).
62. Wu, X. *et al.* Thermally stable, biocompatible, and flexible organic field-effect transistors and their application in temperature sensing arrays for artificial skin. *Adv. Funct. Mater.* **25,** 2138–2146 (2015).
63. Schwartz, G. *et al.* Flexible polymer transistors with high pressure sensitively for application in electronc skin and health monitoring. *Nat. Commun*. **4**, 1859 (2013).
64. Gundlach, D. Organice electronics: Low power, high impact. *Nat. Mater*. **6,** 173–174 (2007).
65. Hong, J. *et al.* Tuning of Ag work functions by self-assembled monolayers of aromatic thiols for an efficient hole injection for solution processed triisopropylsilylethynyl pentacene organic thin film transistors. *Appl. Phys. Lett*. **92,** 143311 (2008).

Acknowledgements

This work was supported in part by the National Natural Science Foundation of China under Grant 61274083 and Grant 61334008, in part by the 863 Program under Grant 2014AA033002, and in part by the Ph.D. Programs Foundation through the Ministry of Education, China, under Grant 20120073110093.

Author Contributions

X.G. conceived the device concept. L.F. and W.T. constructed and characterized the devices. L.F., J.Z. and R.Y. fabricated the sensor tag and conducted the sensing measurements. W.H., Q.L. and R.W. were responsible for the fabrication of circuit board. L.F. and X.G. analyzed the data and wrote the manuscript. X.G. supervised the project. All authors discussed the results.

Additional Information

Supplementary information accompanies this paper at http://www.nature.com/srep

Competing financial interests: The authors declare no competing financial interests.

How to cite this article: Feng, L. *et al.* Unencapsulated Air-stable Organic Field Effect Transistor by All Solution Processes for Low Power Vapor Sensing. *Sci. Rep.* **6**, 20671; doi: 10.1038/srep20671 (2016).